Check for updates

Received: 19 June 2020 | Revised: 9 July 2020 | Accepted: 13 July 2020

DOI: 10.1002/ppap.202000129

FULL PAPER

PLASMA PROCESSES AND POLYMERS

Evidence of ionic film deposition from single-filament dielectric barrier discharges in Ar–HMDSO mixtures

Lars Bröcker | **Gesa S. Perlick** | **Claus-Peter Klages**

Institute for Surface Technology, IOT, Technische Universität Braunschweig, Braunschweig, Germany

Correspondence
Lars Bröcker, Institute for Surface Technology, IOT, Technische Universität Braunschweig, Bienroder Weg 54 E, 38108 Braunschweig, Germany.
Email: l.broecker@tu-braunschweig.de

Please note that the numbering of four formulas and reference [72] were corrected on 2 September 2020 after initial publication.

Abstract

The short residence time of Ar–HMDSO (Ar–hexamethyldisiloxane) gas mixtures rapidly flowing across atmospheric-pressure, glow-type, single-filament dielectric barrier discharges is utilized to accomplish thin-film deposition via a purely ionic route. A comparison of thin-film volumes obtained from profilometry, on the one hand, and from the transferred charge, on the other hand, enables to evaluate the mass of the ions contributing to the film growth. For HMDSO fractions at the lower end of the studied range of molar fractions, 50 ppm, pentamethyldisiloxanyl cations ($Me_3SiOSiMe_2^+$, $PMDS^+$), generated from the monomer via Penning ionization by Ar(1s) species, are mainly responsible for film formation. For HMDSO fractions growing beyond 1,000 ppm, ionic oligomerization processes by reactions of $PMDS^+$ with HMDSO molecules result in a 2.5-fold increase of the average deposited ion mass.

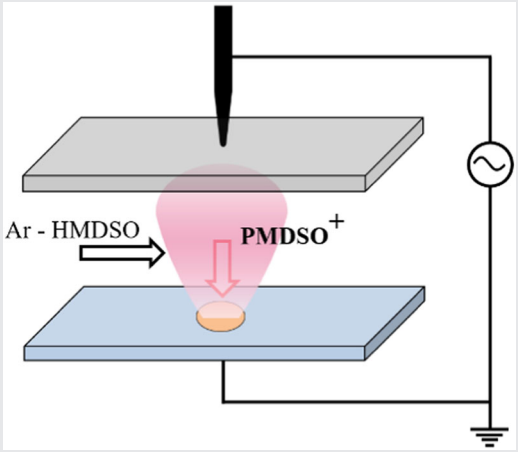

KEYWORDS

atmospheric-pressure glow discharge, dielectric barrier discharge, hexamethyldisiloxane, ion deposition, plasma polymerization, single filament

1 | INTRODUCTION

During the past decades, atmospheric-pressure plasmas have received increasing attention from industry as well as from the scientific community, due to several advantages over low-pressure plasmas, such as the enabling of continuous processes, reduced equipment costs, and scalability.[1] In the field of coating and surface technologies, studies on polymer surface modification as well as plasma-enhanced chemical vapor deposition (PECVD) of thin films by dielectric barrier discharges (DBDs) have been reported in numerous contributions. For the latter

This is an open access article under the terms of the Creative Commons Attribution-NonCommercial-NoDerivs License, which permits use and distribution in any medium, provided the original work is properly cited, the use is non-commercial and no modifications or adaptations are made.
© 2020 The Authors. *Plasma Processes and Polymers* published by Wiley-VCH Verlag GmbH & Co. KGaA

applications, hexamethyldisiloxane (HMDSO) has frequently been employed as a precursor ("monomer") to investigate the deposition process ("plasma polymerization") and film properties, respectively.[2–17]

In contrast to low-pressure PECVD of HMDSO, where the monomer is a major if not the only component of the gas phase,[18–36] carrier gases like argon, helium, or nitrogen are generally essential for atmospheric-pressure plasmas to transport the precursor, with fractions up to 10,000 ppm, into the plasma zone. Whereas noble gases and N_2 are inert when used as carrier gases for thermal CVD, these gases may have a considerable impact on the plasma chemistry in the case of PECVD processes. In the present paper, we will use argon as a carrier gas containing small monomer (M) fractions[1] of HMDSO, $x_M \leq$ 2,000 ppm (=0.2%), to deposit plasma polymers from HMDSO ("pp-HMDSO"). Under these conditions, processes involving a direct electron collision with the monomer are less important than collisions resulting in an energy transfer from Ar atoms in metastable or resonant Ar(1s) states as well as Ar_2 excimers. The reactions of HMDSO with Ar(1s) species result in dissociative ionization (Penning ionization) as well as in dissociation into neutral radicals, with probabilities of 30% and 70%, respectively.[16] For HMDSO fractions up to 200 ppm, Penning ionization is by far the predominant electron source, with a contribution to the total ionization rate of more than 90%.[16] For monomer fractions growing beyond 200 ppm, the contribution of direct electron impact ionization of HMDSO to the total ionization rate increases significantly, but at $x_M = 1{,}500$ ppm, Penning ionization still contributes 63%.[17] Both Penning ionization and electron impact ionization result in the formation of pentamethyldisiloxanyl ($PMDS^+$) ions, $Me_3SiOSiMe_2^{+}$[2], along with methyl radicals, CH_3. Although the ionization of HMDSO plays an important role, ions are often neglected as potential contributors to film formation in plasma polymerization of HMDSO and only neutral radicals are considered.[2,4,8–10,15,33]

In the present study, we are using an asymmetric single-filament DBD (SF-DBD) setup, employing a pin-to-plate electrode arrangement with an insulator-covered pin, to obtain HMDSO plasma polymers deposited exclusively from ions. In literature, studies on SF-DBDs have frequently been performed to gain fundamental knowledge about discharge mechanisms of filamentary DBDs, which is difficult to obtain from conventional DBDs with a large number of filaments distributed in space and time.[37–39]

Ar–HMDSO mixtures generally form uniform glow DBDs over a wide range of x_M, due to the dominance of Penning ionization.[17] The "single-filament" DBDs in these mixtures, obtained in the present study, are of substantial interest, because they represent DBDs with the lowest possible extension in the gas flow direction, typically 0.1 cm. Therefore, the gas residence time, $\tau_{res,s}$, in the plasma zone of SF-DBDs is reduced to around 1 ms at average gas velocities, v_{av}, in the order of 1 m/s. "Macroscopic" DBD reactors used for film deposition with typical lengths of 10 cm, however, will typically have $\tau_{res,m}$ values in the order of 100 ms. This difference is important because the characteristic time for diffusion of neutrals to the walls is mostly in the range 10–100 ms. As an estimate of τ_{diff}, the decay time of the fundamental diffusion mode in a plane sheet with thickness h, $\tau_{diff} = (h^2/\pi^2/D)$, can be used. D is the diffusion coefficient of a species.[40] With the relatively large gap width used in this study, $h = 0.25$ cm, and $D_{HMDSO,Ar} = 0.035\ cm^2/s$,[9] the result is $\tau_{diff} = 0.2$ s. Ion drift times, however, are much smaller than diffusion times: $\tau_{drift} = 0.5\ \mu s$ is obtained, for example, for 0.3-mm distance, a field of $E = 23$ kV/cm (see Section 4 for this choice), and a mobility ($PMDS^+$ in Ar) of $\mu = 2.3\ cm^2 \cdot V^{-1} \cdot s^{-1}$.[41]

A consideration of these time scales shows that in macroscopic reactors, the deposition of neutral fragments from DBD-activated plasma processes largely takes place within the plasma zone, because τ_{diff} and $\tau_{res,m}$ are of comparable magnitude. In our SF-DBDs, in contrast, $\tau_{diff} \gg \tau_{res,s}$; therefore, neutral products cannot deposit in the plasma zone, because they are carried away by convection before reaching the walls. The ion drift process, however, is virtually instantaneous on the residence time scale, because $\tau_{drift} \ll \tau_{res,s}$: Ions will be transported to the surface as soon as they are produced, unaffected by the gas flow. Furthermore, the small residence time in SF-DBDs helps to simplify plasma-chemical mechanisms in the discharge and to avoid or suppress unwanted follow-up processes like the formation of nanoparticles. Also, the monomer depletion is kept small.

The present paper reports the electrical characterization of asymmetric SF-DBDs in Ar–HMDSO with monomer fractions x_M between 50 and 2,000 ppm,[3] as well as the characterization of thin films grown from these gas mixtures, using Fourier-transform infrared spectroscopy (FTIR) in the attenuated total reflectance (ATR) mode, elemental analysis by wavelength-dispersive X-ray spectroscopy (WDXS), and profilometry. One important objective of the paper is to correlate the film volume from profilometric data with the transferred

[1]Monomer fractions in this paper refer to molar fractions.

[2]"Me" stands for the methyl group, CH_3.

[3]Extinction voltages are reported up to $x_M = 3{,}000$ ppm.

16128869, 2020, 11, Downloaded from https://onlinelibrary.wiley.com/doi/10.1002/ppap.202000129 by Technische Informationsbibliothek, Wiley Online Library on [23/01/2025]. See the Terms and Conditions (https://onlinelibrary.wiley.com/terms-and-conditions) on Wiley Online Library for rules of use; OA articles are governed by the applicable Creative Commons License

charge obtained from electrical measurements, to test the hypothesis that film deposition is exclusively due to ion deposition. Besides the named analytical methods, photographs were taken to visualize the plasma shape as it appears in the spectral region of camera sensitivity.

2 | EXPERIMENTAL SECTION

2.1 | Materials

HMDSO (≥98.5%) was obtained from Sigma-Aldrich Chemie GmbH (Steinheim, Germany). Argon (purity 6.0) was from Linde AG, Germany. Silicon wafers of 500-μm thickness with a resistivity ρ of 10–20 Ω·cm were obtained from SIEGERT WAFER GmbH.

2.2 | Instrumentation

PECVD experiments were performed at ambient pressure using a DBD reactor with an asymmetric electrode arrangement, as shown schematically in Figure 1. The high-voltage generator was connected to a sharpened tungsten rod electrode with a diameter of 1.6 mm, glued to a 1-mm borosilicate glass dielectric. Sharpening was done manually with coarse SiC abrasive paper. To fix the tungsten tip and simultaneously avoid the formation of sliding discharges on the glass surface, epoxy glue (RS Pro Quick Set Epoxy Adhesive) from RS Components Ltd. (Corby, UK) was applied. In previous experiments with copper wire, delamination of the epoxy resulted in partial discharges near the tip of the electrode and eventual failure of the setup.[4] Ethanol-cleaned silicon substrates ($2.2 \times 1.0\,cm^2$) were placed on a grounded Al plate, forming a discharge gap of 2.5 mm.[5] To generate Ar–HMDSO mixtures with controlled x_M, argon was fed through a glass bubbler filled with the monomer and kept at a temperature of 20°C, diluted by a second stream of pure Ar. The oxygen concentration in the discharge gap was always kept below 2 ppm, to avoid the formation of inorganic SiO_x-like films.

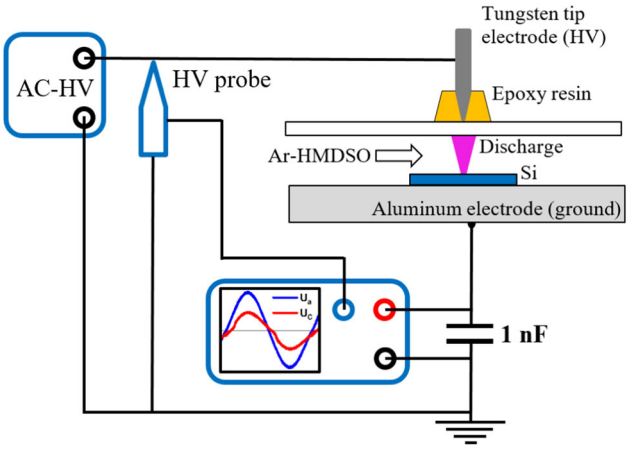

FIGURE 1 The experimental setup. HMDSO, hexamethyldisiloxane; HV, high voltage

Figure 1 also shows the equivalent circuit of the DBD arrangement. The discharge was powered by a high-voltage generator from SOFTAL electronics GmbH (Hamburg, Germany), model 7010R, delivering a sinusoidal voltage output. For electrical characterization of the discharge, the voltage applied to the discharge arrangement, $U_a(t)$, and the transferred charge $q(t)$ were measured using a high-voltage probe (Tektronix P6015A) and capacitor (1 nF) in series, respectively. An oscilloscope (Tektronix MDO3052) was used to monitor $U_a(t)$ and the voltage drop $U_C(t)$ at the capacitor to calculate discharge currents, I_d, the dissipated energy, E_g, and the deposited volume via charge transfer V_t. The capacity of the DBD setup without discharge was determined using an LCR meter, resulting in 2.05 pF.

FTIR–ATR measurements were performed by means of a Spotlight 200i FTIR Microscopy System (PerkinElmer, Shelton, CT), using a germanium ATR crystal with an average angle of incidence of 38°, an aperture of $100 \times 100\,\mu m^2$, and a spectral resolution of $4\,cm^{-1}$. Averaging was performed over 256 scans. The elemental analysis was done by WDXS on a Cameca SX50 (CAMECA, Gennevilliers, France), using an electron energy of 5 keV. For profilometry measurements, a DektakXT (Bruker, Champs-sur-Marne, France) was used with an operating force of 1 mg. As shown below for one example (see Figure 6), the deposits have virtually circular symmetry and the deposit thickness d depends only on the radial distance r from the film center. Scans were carefully performed through the center of the bell-shaped deposits where $d(0) = d_{max}$, in gas flow direction and across, respectively, to obtain four independent measurements of $d(r)$. The deposit volume V_p was calculated from the averaged $d(r)$ data by numerical integration of the product, $d(r) \times 2\pi r$ over r, in the limits from $r = 0$ to an upper value r_{max}, where $d(r_{max})$ was virtually zero. In certain regions, d may be in error by

[4]Weak adhesion strength of copper/epoxy joints, for example, in printed circuit boards, has been an issue for decades, see, for example, the review reported in Nothdurft et al.[42]

[5]The simple equation for the spreading resistance of a disc-shaped contact on a thick conductor,[43] $R_S = \rho/(4a) \approx 100\,\Omega$, which can be calculated from the Si wafer resistivity ρ and the diameter of the contact area between Si and the filament, $2a$ (see below), results in a negligible voltage drop (<1 V) in the Si substrate, owing to the small discharge currents of typically <1 mA. Although the actual situation is not exactly represented, this calculation gives at least an order-of-magnitude estimate and shows that the substrate may be considered as a near-perfect conductor.

16128869, 2020, 11, Downloaded from https://onlinelibrary.wiley.com/doi/10.1002/ppap.202000129 by Technische Informationsbibliothek, Wiley Online Library on [23/01/2025]. See the Terms and Conditions (https://onlinelibrary.wiley.com/terms-and-conditions) on Wiley Online Library for rules of use; OA articles are governed by the applicable Creative Commons License

approximately −10% because the stylus sometimes left scratches in the film over the first and last 50 μm of the profile. Finally, photographs of the plasma shape were taken using a Canon EOS 7D Mark II camera at 10-s exposure time.

2.3 | Procedures

The high-voltage generator was used in continuous wave (cw) mode, operating at a frequency of 19 kHz. An excitation voltage amplitude U_{a0} of 1.75 ± 0.05 kV was applied for all film deposition experiments presented here. The total gas flow was set to 1,650 cm^3/s at standard temperature and pressure to obtain an average gas flow velocity v of 50 cm/s through the discharge gap; the duration of the experiments was varied, in inverse proportion to x_M, between 450 s for $x_M = 50$ ppm HMDSO and 11.25 s for $x_M = 2{,}000$ ppm, and the resulting film thickness d_{max} was between 1 and 4 μm. Owing to the small volume of the high-field region between the electrodes, the discharge ignition was sometimes substantially delayed due to the lack of start electrons. For this reason, the extinction voltage $U_{a0,ex}$ was measured as a function of x_M up to $x_M = 3{,}000$ ppm, to obtain an additional characteristic of the discharge. For these experiments, the discharge was ignited and U_{a0} was decreased until the discharge became extinct again, that is, any discharge signal on the oscilloscope was no longer visible.

Before igniting the discharge, the reactor was purged with the process gas mixture for 150 s. After film deposition, analyses of the samples were performed within 8 hr.

3 | RESULTS

3.1 | Electrical characterization and visual appearance of the discharge

3.1.1 | Extinction voltages

Results of extinction voltage ($U_{a0,ex}$) measurements are shown in Figure 2, together with selected examples of DC sparking voltages U_s taken from the work of Heylen et al.[44–46] on the Penning effect of mixtures of Ar with hydrocarbons. The qualitative dependence of these voltages as a function of HMDSO and hydrocarbon fractions, x_M and x_H, respectively, is quite similar: A rapid decrease of the voltage for small fractions of the added molecular species, with a minimum near 300 ppm, is followed by a slow increase for larger fractions. The HMDSO data suggest a short plateau region for x_M between 200 and 500 ppm, whereas a corresponding range of x_H with constant U_s is not observable, owing to the sparsity of data points. It should be noted that for Ar-HMDSO the applied voltage, still containing the contribution of the voltage drop across the glass dielectric, was used, whereas the hydrocarbon data were obtained with two metal electrodes.[46] This explains a part of the differences between absolute values of $U_{a0,ex}$ for HMDSO and U_s for pentane[44] or octane.[45] In a previous paper by Loffhagen et al.,[16] gap voltages at ignition, $U_{g,ign}$, were reported for DBDs in Ar–HMDSO with 8-cm^2 electrodes for $x_M \leq 200$ ppm, also showing a steep decrease up to approximately 50 ppm, followed by a more gradual decline up to 200 ppm. An extraction of gap voltages, $U_{g0,ex}$, in the present case is not straightforward, owing to the strongly inhomogeneous electric field. A corresponding analysis is planned for a future publication.

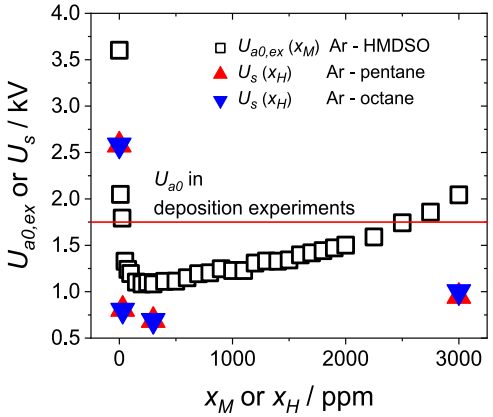

FIGURE 2 Extinction voltages for different fractions x_M of hexamethyldisiloxane (HMDSO) in Ar (open squares). The red horizontal line at 1.75 kV indicates the applied voltage in further experiments. Red and blue triangles show sparking voltages for Ar with additions of pentane[44] and octane,[45] respectively

3.1.2 | Discharge currents

Discharge currents $I_d(t)$ were determined from the voltage drop $U_C(t)$ at the capacitor with a capacity of the DBD arrangement of 2.05 pF, following Pipa and Brandenburg.[47] The results are displayed in Figure 3.

In general, both half cycles show that the current peaks become broader and smaller with monomer fractions increasing from 50 up to 250 ppm. With a further increase of x_M, the current peaks become narrower and taller again. Regarding the negative half cycle (Figure 3b), the discharge duration, taken as the full width at half maximum, increases from approximately 1.0 μs (50 ppm) to a maximum of 1.2 μs (250 ppm) and

16128869, 2020, 11, Downloaded from https://onlinelibrary.wiley.com/doi/10.1002/ppap.202000129 by Technische Informationsbibliothek, Wiley Online Library on [23/01/2025]. See the Terms and Conditions (https://onlinelibrary.wiley.com/terms-and-conditions) on Wiley Online Library for rules of use; OA articles are governed by the applicable Creative Commons License

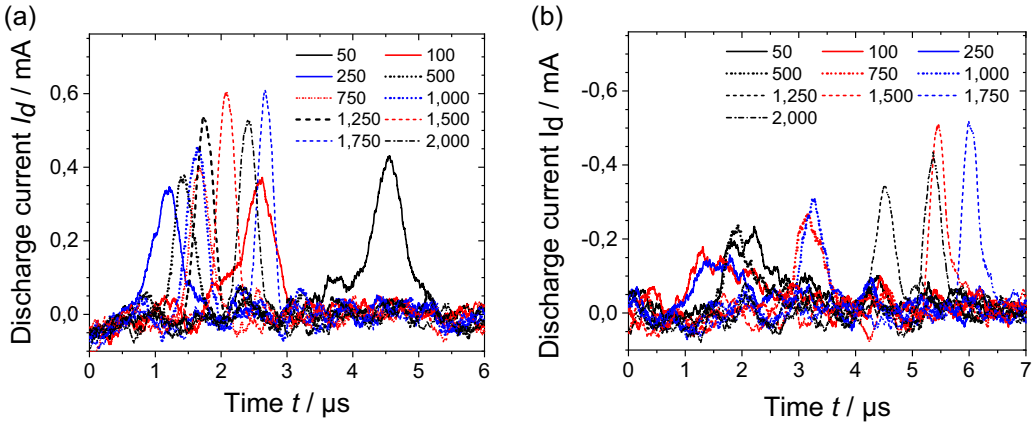

FIGURE 3 Discharge currents $I_d(t)$ for a positive (a) and a negative (b) half cycle, respectively, at $U_{a0} = 1.75$ kV, for monomer fractions from 50 to 2,000 ppm (see legends)

declines to a value of 0.4 µs (2,000 ppm). Similar values are obtained for the positive half cycle in Figure 3a.

Another effect, particularly seen in the positive half cycle, is that current peaks occur earlier with HMDSO fractions rising up to approximately 250 ppm, whereas a shift to larger t can be observed with x_M growing beyond 250 ppm. Broader and less intensive peaks indicate a bigger impact of Penning ionization, in agreement with the abrupt decline of the excitation voltage with small HMDSO admixtures (see also Figure 2). Monomer fractions above 250 ppm lead to a decrease of Penning ionization contribution to the total ionization rate, and there is also a decrease in the total ionization rate. Hence, current peaks become thinner and taller again. The shift of current peaks follows the trend of the extinction voltage in Figure 2. Parallel to the decrease of the extinction voltage for small HMDSO admixtures, the gap voltage decreases and the current peaks occur earlier. For even larger monomer concentration, the opposite effect is observed. A more detailed analysis must be set aside for a future publication in conjunction with numerical modeling.

3.1.3 | Dissipated energy

The electrical energy dissipated in the single-filament gas discharge E_g per period T is calculated from the enclosed area of voltage–charge plots ($q(t)$ vs. $U_a(t)$), using the following equation:

$$E_g = C_c \int_{t_0}^{t_0+T} U_c(t)\, dU_a(t). \quad (1)$$

Figure 4 shows E_g as a function of x_M for $U_{a0} = 1.75$ kV. For every data point, nine measurements were averaged. Vertical bars are standard deviations. The trend of E_g qualitatively resembles that of the extinction voltage in Figure 2, with a steep decrease toward a minimum, followed by a gradual increase. Different from the behavior of $U_{a0,ex}$, E_g has its minimum at a significantly larger monomer fraction, $x_M = 500$ ppm. The corresponding curve for a large-area DBD (LA-DBD) presented in Loffhagen et al.[17] for x_M up to 1,600 ppm shows a less pronounced minimum region between 200 and 500 ppm.

3.1.4 | Visual discharge appearance

The photographs displayed in Figure 5a–j show the shapes of the plasma, as seen by the naked eye, for different admixtures of HMDSO in argon. At small x_M, the asymmetry of the reactor configuration results in the plasma shape of an inverted truncated cone with a base diameter d_b of 4.5 mm on the upper dielectric wall, in spite of the sharp tip electrode on the other side of

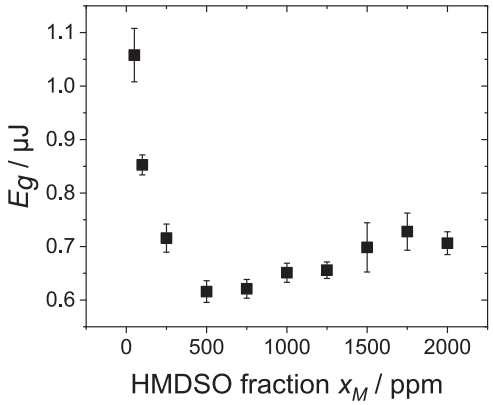

FIGURE 4 Energy dissipated per period, E_g, as a function of the hexamethyldisiloxane (HMDSO) fraction x_M

16128869, 2020, 11, Downloaded from https://onlinelibrary.wiley.com/doi/10.1002/ppap.202000129 by Technische Informationsbibliothek, Wiley Online Library on [23/01/2025]. See the Terms and Conditions (https://onlinelibrary.wiley.com/terms-and-conditions) on Wiley Online Library for rules of use; OA articles are governed by the applicable Creative Commons License

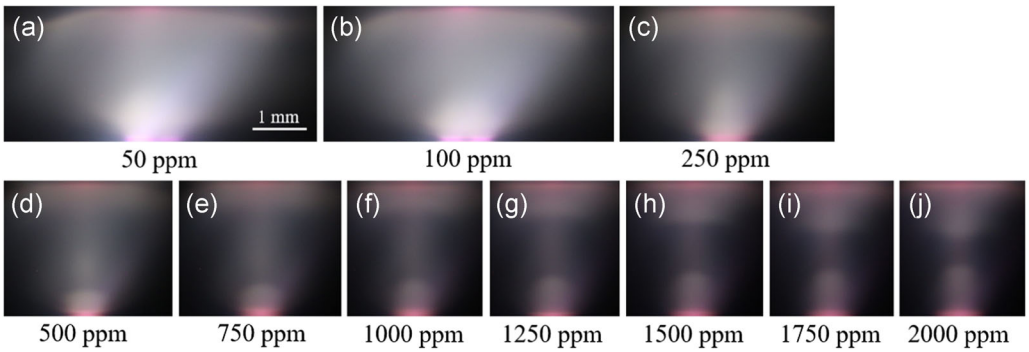

FIGURE 5 Photographs of the plasma shape at $U_a = 1.75$ kV for 50 ppm $< x_M <$ 2,000 ppm. The dielectric wall covering the tip electrode is at the top. Letters a) to j) indicate different HMDSO fractions used for plasma polymerization

the glass plate. The luminous intensity grows toward the lower conductive wall. The circular contact area with the lower electrode decreases from 1.3 to 0.5 mm at 500 ppm and beyond.

The total brightness of the discharge apparently decreases up to a monomer fraction of approximately 500 ppm, parallel to the decrease of the dissipated energy E_g. For HMDSO fractions larger than 500 ppm (Figure 5d–j), the discharge is divided by a weakly glowing gap that becomes smaller with larger monomer admixture. The brighter glowing regions, extending 600–900 μm from the walls in the vertical direction, are probably the negative glows adjacent to the cathode fall regions developing transiently on the lower electrode and the upper dielectric during the discharge processes in the positive and negative half cycle, respectively. A more detailed analysis is planned for a future publication, based on spatially and phase-resolved studies of the optical discharge emission.

3.2 | Film volumes from profilometric and electrical measurements

Owing to the relatively small ion drift time, the axial symmetry of the discharge and the lack of significant monomer depletion during passage through the discharge, all deposits obtained for the x_M range in this study have nearly perfect circular symmetric thickness profiles and interference patterns, as shown in Figure 6.

The volume of pp-HMDSO deposited per cycle on the lower conducting electrode is calculated from the transferred charge, assuming that deposition is solely due to ions, and by making assumptions with respect to the molecular mass of the ions and the density of the plasma polymer. The result, V_t, is then compared with the volume calculated from the profilometric measurement (V_p, see Section 2). The transferred charge, q_t, is determined from the measurements that were already made to calculate E_g, see Equation (1), displayed as voltage–charge plots. The mass deposition due to the charge transfer, m_t, is calculated from the following equation:

$$m_t = \eta \times (q_t/F) \times M_{PMDS^+}. \quad (2)$$

In Equation (2), F is the Faraday constant, 96,485 As/mol, and it is assumed that only $PMDS^+$ ions with a molecular mass $M_{PMDS+} = 147.3$ g/mol are contributing to the deposition. The sticking coefficient η is the probability that the PMDS radical left after discharging the ion will remain on the surface. Here, $\eta = 1$ will be assumed;

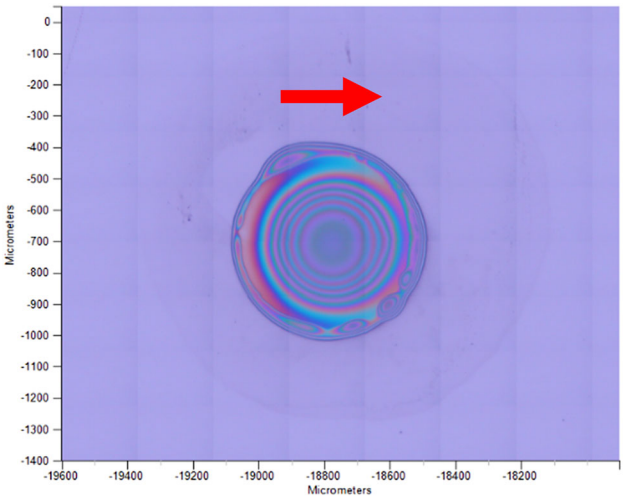

FIGURE 6 Micrograph of the interference pattern of a film deposited at $x_M = 1{,}000$ppm. The picture was taken using the camera of the Spotlight 200i FTIR Microscopy System. The red arrow indicates the gas flow direction

16128869, 2020, 11, Downloaded from https://onlinelibrary.wiley.com/doi/10.1002/ppap.202000129 by Technische Informationsbibliothek, Wiley Online Library on [23/01/2025]. See the Terms and Conditions (https://onlinelibrary.wiley.com/terms-and-conditions) on Wiley Online Library for rules of use; OA articles are governed by the applicable Creative Commons License

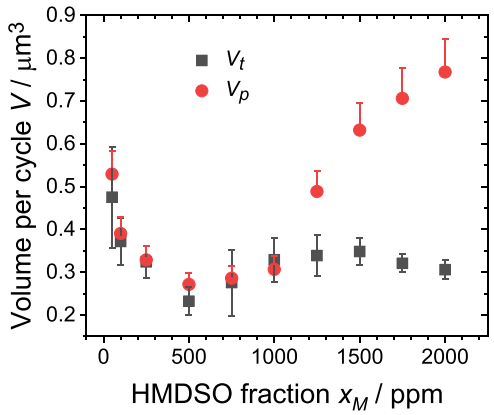

FIGURE 7 Thin-film volumes calculated from the transferred charge, V_t (black squares), and from profilometric measurements, V_p, (red circles). The positive red error bars account for possible errors in thickness measurements, resulting in too low values, see Section 2.3. HMDSO, hexamethyldisiloxane

this assumption will be discussed in Section 4.2. V_t is calculated from m_t by dividing by the mass density of the film, ρ. In the absence of measurements of ρ, it appears reasonable to adopt the average of values reported in the literature for pp-HMDSO films obtained by low-pressure plasma polymerization at a relatively low power. A value of 1.1 g/cm^3 (10% beyond the mass density of polydimethylsiloxane), resulting from the data in References [27,36], will be used here. In Figure 7, the obtained volumes are shown as black squares and compared with V_p from profilometry (see Section 2.2), shown as red circles.

Up to an HMDSO fraction of 1000 ppm, the volumes are virtually identical, within the range of experimental errors. The divergence of V_t and V_p beyond $x_M = 1{,}000$ ppm is more obvious in Figure 8, showing the ratio $R_V \equiv V_p/V_t$.

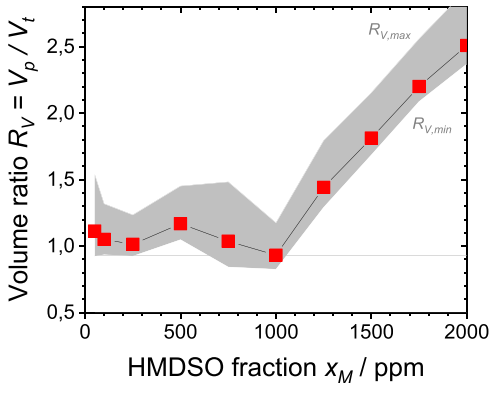

FIGURE 8 Ratio R_V of the deposited volumes via profilometric measurements, V_p, and calculated from the transferred charge, V_t. Grey area indicates the maximum and minimum error. HMDSO, hexamethyldisiloxane

The observation that R_V is close to one for small x_M and the overall increase of R_V to 2.5 at $x_M = 2{,}000$ ppm will be discussed below in terms of ion deposition of $PMDS^+$ ions for $x_M \ll 1{,}000$ ppm (Section 4.2) and an ionic oligomerization process for larger monomer fractions (Section 4.3).

3.3 | Infrared (IR) spectra

Figure 9a–c shows the results of unpolarized FTIR–ATR microscopic measurements using a Ge ATR crystal with 38° reflection angle. The spectra were taken at the center of the deposited films; no systematic variations were observed when other positions on a film were measured. Table 1 shows peak positions ν of films deposited from the SF-DBD for the whole x_M range, compared with general peak positions given in the book by Socrates[49] or the article about IR spectroscopy of silicones by Anderson.[48] No systematic peak shifts with x_M were observed within the studied concentration range. However, there was a substantial variation in relative peak intensities, as shown in Figure 9c.

In Figure 9a, a characteristic spectrum of a pp-HMDSO sample deposited by a conventional LA-DBD[13] is compared with two spectra taken from samples from the present study. The spectra are normalized to have the same band heights for the $\delta^a(CH_3)$ vibration, which appears at approximately 1,252 and 1,253 cm^{-1} for SF-DBD samples obtained with the four highest and three lowest x_M values, respectively. In the LA samples, the maximum is also at 1,253 cm^{-1}. This normalization gives the ν^a(Si–O–Si) bands virtually the same band areas. Maxima of these bands are downshifted by about 10 cm^{-1} from 1,030 cm^{-1} in the LA case to the range of $1{,}020 \pm 4$ cm^{-1} for all SF samples. This peak position is at the lower end of the range (1,020–1,080 cm^{-1}) observed in low-pressure-deposited pp-HMDSO[19,20,22,23,25,26,32] grown without substrate bias,[6] but it is not unusual for films grown at atmospheric pressure.[8] The LA spectrum has the typical "silicone-like" appearance, as it can also be seen in References [8,14]. The main differences in the SF samples are the peaks at 2,118 and at 1,353–1,355 cm^{-1}, related to Si–H and Si–CH_2–Si moieties, respectively, which do not appear in permethylated polysiloxanes.

Figure 9b shows the region of C–H and Si–H stretching vibrations for two samples deposited with $x_M = 250$ and 1,750 ppm, respectively. The 3,000–2,850 cm^{-1} region is dominated by ν^a and ν^s of CH_3, and corresponding peaks of CH_2 appear in some spectra with a smaller

[6]In films grown on a biased substrate, this band can be seen at 1,000 cm^{-1}[31] or 1,010 cm^{-1}.[35]

16128869, 2020, 11, Downloaded from https://onlinelibrary.wiley.com/doi/10.1002/ppap.202000129 by Technische Informationsbibliothek, Wiley Online Library on [23/01/2025]. See the Terms and Conditions (https://onlinelibrary.wiley.com/terms-and-conditions) on Wiley Online Library for rules of use; OA articles are governed by the applicable Creative Commons License

intensity. There is no clear trend with x_M for the intensities of these vibrations as well as the Si–H stretching vibration bands at 2,118 cm^{-1}. It should be noted that there is an additional Si–H component near 1,070–1,080 cm^{-1} in the 1,750-ppm spectrum, which appears in all samples with $x_M > 1{,}000$ ppm.

The most obvious differences within the SF-DBD samples can be seen in Figure 9c if spectra for $x_M > 750$ ppm are compared with lower x_M results. The occurrence of an additional absorbance maximum at 767 ± 1 cm^{-1} in the former spectra is tentatively attributed to the presence of Si–Me_1 moieties in these samples.

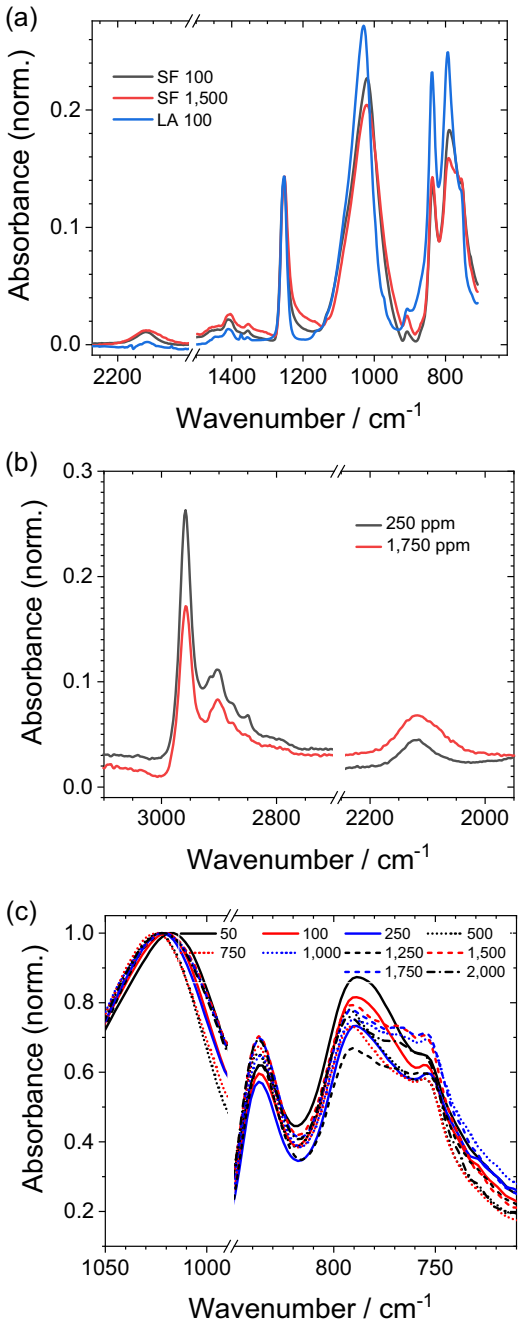

TABLE 1 FTIR peak positions, assignments, and literature data

ν (cm^{-1})	Assignment	Literature
2,956–2,958	$\nu^a(CH_3)$ in $SiMe_x$	2,970[48]
2,921–2,914	$\nu^a(CH_2)$ aliph.	2,940–2,915[49]
2,903–2,899	$\nu^s(CH_3)$ in $SiMe_x$	2,910[48]
2,877–2,873	$\nu^s(CH_2)$ aliph.	2,870–2,840[49]
2,120	$\nu(SiH_x)$	2,250–2,100[49]
1,408	$\delta^a(CH_3)$ in $SiMe_x$	1,390–1,440[48]
1,355–1,353	$\delta(CH_2)$ in $SiCH_2Si$	1,380–1,340[48]
1,253–1,252	$\delta^s(CH_3)$ in $SiMe_x$	1,280–1,240[48]
1,024–1,016	ν^a(Si–O–Si)	1,070–1,040[48]
909–906	ν(Si–O) in SiOH	955–830[49]
837–835	ν(Si–C), $\rho^a(CH_3)$ in $SiMe_3$	845[48]
793–790	ν(Si–C), $\rho^a(CH_3)$ in $SiMe_2$	805[48]
768–766	ν(Si–C), $\rho(CH_3)$ in $SiMe_1$	775[48]
754	ν(Si–C), $\rho^s(CH_3)$ in $SiMe_3$	760[48]

It should be noted that ν(O–H), typically around 3,400 cm^{-1}, and ν(C═O), at 1,710–1,730 cm^{-1}, are virtually absent in all spectra, owing to the low oxygen impurity content in the Ar–HMDSO mixture.

3.4 | WDXS analysis

In the absence of knowledge of density and hydrogen content, absolute weight or atomic percentages of the heavy elements cannot be measured separately using WDXS. Therefore, Figure 10 shows the ratios of atomic contents [C]/[Si] and [O]/[Si], respectively, for HMDSO admixtures between 50 and 2,000 ppm. Data from the 500-ppm sample are excluded as outliers.

The decrease of the [C]/[Si] is in agreement with a presumed ionic oligomerization process, increasing with the increase in x_M, as suggested in Section 3.2. The corresponding ratios in the pentamethyldisiloxanyl ($PMDS^+$, $Me_3SiOSiMe_2^+$), heptamethyltrisiloxanyl ($HepMTrS^+$, $Me_3SiOSiMe_2OSiMe_2^+$), and nonamethyltetrasiloxanyl ($NMTeS^+$, $Me_3SiO(SiMe_2O)_2SiMe_2^+$) cations, respectively, the latter as a result of formal addition of one or two dimethylsiloxane units, $(CH_3)_2Si{=}O$, are shown in Figure 10 as horizontal lines. The [O]/[Si] ratio in these ions is 0.5, 0.67, and 0.75, respectively. See Section 4 for further discussion.

16128869, 2020, 11, Downloaded from https://onlinelibrary.wiley.com/doi/10.1002/ppap.202000129 by Technische Informationsbibliothek, Wiley Online Library on [23/01/2025]. See the Terms and Conditions (https://onlinelibrary.wiley.com/terms-and-conditions) on Wiley Online Library for rules of use; OA articles are governed by the applicable Creative Commons License

4 | DISCUSSION

In previous studies of film deposition from atmospheric-pressure discharges containing HMDSO or related silicon-containing precursors, neutral radicals have frequently been assumed to be the growth species.[2,4,8–10,15] However, for parallel-plate radio-frequency (RF) plasma deposition from siloxanes at low pressure, a detailed ionic mechanism of film formation was postulated by Vasile and Smolinsky[18] in 1972, including the possibility of cationic gas-phase oligomerization before eventual neutralization of the ions at the wall and incorporation of the resulting radicals into the growing film. The mechanism of cationic film formation and its role in PECVD have more recently been studied by Short and colleagues, using inductively coupled RF plasmas[28,34] and, with a group at the University of Illinois at Chicago, using deposition from a mass-filtered beam of hyperthermal $PMDS^+$ ions.[50,51] Michelmore et al.[34] showed convincingly that $PMDS^+$ ions contribute substantially to the deposited mass in PECVD activated by an RF plasma. In the following discussion, it will be shown that the same ions also play a role in DBD-activated PECVD at atmospheric pressure.

FIGURE 9 (a) Fourier-transform infrared spectroscopy–attenuated total reflectance (FTIR–ATR) spectra of samples prepared with 100- or 1,500-ppm hexamethyldisiloxane (HMDSO) using single-filament dielectric barrier discharge (SF-DBD; black, red) and large-area DBD (blue), respectively. The latter spectrum (polypropylene [PP] substrate subtracted, diamond ATR, 51°, s-polarized) from the work by Philipp et al.[13] is from a 0.4-μm-thick sample, deposited 3 cm behind the leading edge of the plasma zone with $U_{a0} = 4$ kV. Features at 2,161 and 1,371 cm^{-1} are from diamond and PP, respectively. (b) A comparison of FTIR–ATR spectra of samples prepared with 250- and 1,750-ppm HMDSO, respectively, in the region of C–H and Si–H stretching vibrations. The maximum absorbance of the spectra in the low wavenumber range was normalized to 1. It should be noted that there exist peaks of CH_2 stretching vibrations at 2,914 and 2,849 cm^{-1}, respectively, in the 250-ppm spectrum and the shoulder near 2,080 cm^{-1} in the 1,750-ppm spectrum. (c) Details of FTIR–ATR of all samples in the wavenumber region below 1,050 cm^{-1}. A linear background was manually subtracted from raw spectra between 1,160 and 600 cm^{-1}. Then the maximum absorbance in the shown range was normalized to 1. It should be noted that there is a sudden increase of intensity at 768 cm^{-1}, relative to the 790-cm^{-1} absorbance for $x_M \geq 1{,}000$ ppm (the legend shows x_M/ppm)

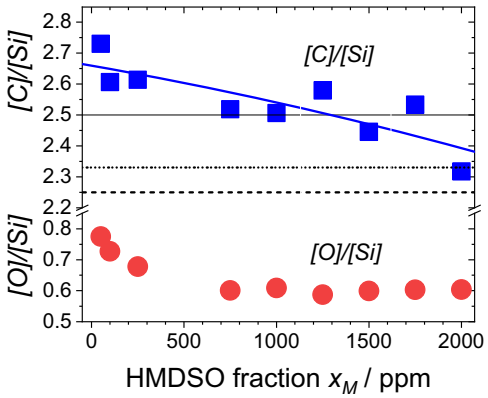

FIGURE 10 Atomic percent ratios [C]/[Si] and [O]/[Si], respectively, for the films deposited with hexamethyldisiloxane (HMDSO) fraction between 50 and 2,000 ppm. Horizontal lines indicate the [C]/[Si] ratios in the pentamethyldisiloxanyl (compact line), heptamethyltrisiloxanyl (dotted), and nonamethyltetrasiloxanyl ions (dashed), respectively. The blue curve is a quadratic fit to the [C]/[Si] data

4.1 | Production of $PMDS^+$ by Penning ionization

In several experimental results presented in Section 3, signatures of a strong Penning effect can be detected: The addition of a small amount of HMDSO to Ar results in a steep decline of extinction voltages $U_{a0,ex}$ (Figure 2), in earlier discharge ignition in I_d curves (Figure 3), a decrease of energy dissipation E_g (Figure 4), and a diffuse visual appearance, typical of a glow discharge (Figure 5). The initial steep decline of $U_{a0,ex}$ as a function of x_M follows the corresponding dependence of the sparking voltages $U_s(x_M)$ in mixtures of Ar with hydrocarbons.[44–46] According to numerical simulations by Loffhagen et al.,[16,17] 30% of the collisions of excited argon species with HMDSO molecules lead to Penning ionization according to Equation (1), whereas neutral dissociation products are formed in 70% of such collisions.

$$Ar^* + HMDSO \rightarrow Me_3SiOSiMe_2^+ + Me + Ar(1p_0) + e. \quad (R1)$$

The hypothesis that $PMDS^+$ is virtually the only product of the Penning ionization is motivated by reports that (a) it is the only ion that can be produced by electron collisions with HMDSO at energies below 16 eV[52] and (b) it is the main product when HMDSO is ionized by reaction with metastable $Ar(^3P_2)$ atoms.[53] The additional channel for electron production via Equation (R1) requires a substantially smaller reduced field than the ionization of Ar, resulting in the

16128869, 2020, 11, Downloaded from https://onlinelibrary.wiley.com/doi/10.1002/ppap.202000129 by Technische Informationsbibliothek, Wiley Online Library on [23/01/2025]. See the Terms and Conditions (https://onlinelibrary.wiley.com/terms-and-conditions) on Wiley Online Library for rules of use; OA articles are governed by the applicable Creative Commons License

observed decrease of extinction and ignition voltages, as well as of E_g.

The main contributors to the reaction (R1) are Ar atoms in resonant or metastable Ar(1s) states. A minimum extinction voltage as a function of x_M is reached when virtually all Ar(1s) atoms are consumed by energy transfer to HMDSO molecules, transforming the monomer into ions or neutral products. This situation requires that the rate of these reactions becomes significantly—at least three times—larger than the rates of competing decay processes of Ar(1s). With a rate coefficient of 5×10^{-10} cm^3/s for reactions of Ar (1s) with HMDSO[16] and an average frequency of 5.5×10^5 s^{-1} of competing monomer-independent decay processes of Ar(1s),[15] a monomer density of approximately 3.3×10^{15} cm^{-3} ($x_M = 140$ ppm) is required for minimal extinction voltage, which is in rough agreement with the experiment.

The increase of extinction voltage at x_M values beyond the minimum region can be attributed to a decrease in the mean electron energy by the addition of HMDSO, resulting in a decreased generation of Ar* species, similar to the situation for Ar–hydrocarbon mixtures.[54] A much more detailed discussion of the energy dissipation in Ar–HMDSO DBDs can be found in a recent publication.[17]

4.2 | Film formation by deposition of PMDS$^+$

The circular symmetric thickness profiles of the deposited films, as shown in Figure 6, cannot be explained by deposition of neutrals, due to the very small ratio of gas residence and wall diffusion time, $t_{res.s}/t_{diff} \approx 0.005$, that is, neutral species are carried out of the discharge zone by convection before reaching the wall by diffusion. The alternative explanation that intact HMDSO molecules are attached to the surface "activated" by the plasma is not very likely in view of the chemical nature of HMDSO. The monomer cannot be attached or polymerized via a radical mechanism. However, more important is the good agreement, for $x_M < 1{,}000$ ppm, of film volumina calculated profilometrically and from the transferred charge, assuming that PMDS$^+$ ions, formed in reaction (R1), arrive at the wall without further transformation by reaction with HMDSO (see Figures 7 and 8).

Although the FTIR spectra of the deposits shown in Figure 9a,b have, prima facie, an "organosiloxane-like" overall appearance, a closer examination reveals two vibrational bands, ν(Si–H) at 2,120 cm^{-1} and $\delta(CH_2)$ in Si–CH_2–Si moieties at $1{,}354 \pm 1$ cm^{-1}, which cannot be explained in simple chemical terms from the structure of the PMDS$^\bullet$ radical. This species should be formed by neutralization of the cation shortly—in the order of a few Å—before wall contact. It is important to note that these moieties cannot have been formed in the gas phase, but they must be the result of reactions taking place during the incorporation of PMDS$^\bullet$ in the growing film. At present, deposit sizes in the submillimeter range preclude X-ray photoelectron spectroscopy (XPS) measurements with the available instrumentation and a better-founded analysis of the bonding situation. For a future publication, XPS spectra are planned to be taken from larger area samples that are grown using a line electrode arrangement. It can be assumed, however, that it is similar to that of films deposited from hyperthermal PMDS$^+$ ions.[50,51] Interestingly, XPS of these polymers reveals a range of silicon binding environments, Si(–C/H), Si(–O_1), Si(–O_2), (Si–O_3), and Si(–O_4)[7] in the ratios of approximately 12:48:29:7:4 for 15-eV ion kinetic energy,[51] whereas the PMDS$^+$ ion has only Si(–O_1). The compositions of films prepared in the present study have a quite similar composition like those obtained by Michelmore et al.[34]: Elemental analysis results reported in the Supporting Information to the author's report about low-pressure PECVD of pp-HMDSO, averaged over three samples grown at the lowest power, 4 W (21% Si, 18% O, 61% C), are virtually identical to the data measured in this study at $x_M = 50$ ppm (22% Si, 17% O, 61% C).

Currently, one can only speculate about the mechanism of film growth under the conditions of SF-DBD. It seems reasonable to assume that the PMDS$^+$ ions will be neutralized near or at the surface[56] by electrons that have been left on the insulating film from the previous discharge with opposite polarity.[57] Electrons are trapped on silicone rubber with binding energies <1 eV.[58] The energy released upon the recombination of PMDS$^+$ with a free electron is not known,[8] which probably will be not very different from the ionization energy of the trimethylsilyl radical, 6.5 eV.[60] The kinetic energy of the ions accelerated in the transient cathode fall, by comparison, is less; an estimation with an equation in the monography by Raizer[61] results in <1 eV. A net energy of approximately 6 eV will, therefore, be transferred to vibrational degrees of freedom, which should lead to splitting of an Si–O bond if the energy is not dissipated in the solid. There are two imaginable possibilities:

[7] These are Si centers N, M, D, T, and Q in the useful notation, in which the letters correspond, respectively, to zero-, mono-, di-, tri-, and quadruply oxygen-bonded R_xSiO_y, where $y = (4 - x)/2$[55]

[8] According to measurements by Jauberteau and Jauberteau,[59] about 20 eV is required to ionize the PMDS$^\bullet$ radical. However, this process possibly results in an excited state of the cation.

16128869, 2020, 11, Downloaded from https://onlinelibrary.wiley.com/doi/10.1002/ppap.202000129 by Technische Informationsbibliothek, Wiley Online Library on [23/01/2025]. See the Terms and Conditions (https://onlinelibrary.wiley.com/terms-and-conditions) on Wiley Online Library for rules of use; OA articles are governed by the applicable Creative Commons License

$$Me_3SiOSiMe_2^+ + e^- \Rightarrow Me_3SiO^\bullet + |SiMe_2 (\Leftrightarrow H(Me)Si{=}CH_2), \quad \text{(R2a)}$$

$$Me_3SiOSiMe_2^\bullet \Rightarrow Me_3Si^\bullet + O{=}SiMe_2. \quad \text{(R2b)}$$

A dissociative recombination of $PMDS^+$ with free electrons in the gas phase,[62] a process virtually excluded in DBDs due to the small electron densities, has been shown to follow channel (R2a), resulting in trimethylsiloxy radicals and dimethylsilylene, $|SiMe_2$, which can equilibrate with hydridosilene $H(Me)Si{=}CH_2$.[63]

The alternative dissociation channel (R2b), resulting in the formation of the trimethylsilyl radical, Me_3Si, and dimethylsilanone, $Me_2Si{=}O$, was postulated to explain the product formation during photolysis of HMDSO using an ArF laser (193 nm, 6.4 eV), which was assumed to proceed via photodissociation of the precursor into $PMDS^\bullet$ and $Me^\bullet$.[64] Similar to the multiphoton IR laser photolysis of HMDSO, substantial redistribution (or "scrambling") of the substituents on silicon atoms takes place, along with the formation of Si–H as well as $Si–CH_2–Si$ moieties.[65] The same is observed upon pyrolysis of a gel obtained by cohydrolysis of dimethyldiethoxysilane and tetraethoxysilane. Possible redistribution reactions, in the nomenclature introduced above, between Si units are as follows: $D + Q \rightarrow 2\,T$, $2\,D \rightarrow M + T$, and $D + T \rightarrow M + Q$.[66]

It is interesting to note in this context that the ion $Me_3SiOSiMe_2^+$ has been playing an important role in mass spectrometric investigations of low-energy collisions of molecular ions at molecular solids (see the reviews of this topic in References [55,67]). On surfaces of fluorinated self-assembled monolayers (F-SAMs), with an estimated ionization energy of 13 eV, $Me_3SiOSiMe_2^+$ ions with a kinetic energy of approximately 10 eV can "land softly," that is, as an intact ion, whereas the closely related ion $ClCH_2Me_2SiOSiMe_2^+$ shows "dissociative landing" under loss of 2C4H, resulting in an ion with the sum formula $C_3H_{10}OSi_2Cl^+$. The estimated fraction of kinetic collision energy converted to the internal energy of these ions is typically only 20%, and the conversion of the ions into radicals by charge exchange with the substrate is precluded by its large ionization energy.[68,69][9] In contrast, the trimethylsilyl cation, $Si(CH_3)_3^+$, which should play a central role in plasma polymerization from Ar–tetramethylsilane mixtures, can show "reactive landing" if deposited with 15 eV on an SAM surface with terminal OH groups, resulting in hydrophobic surface modification.[70]

A final comment should be made on the assumption, made above in Equation (2), that the sticking coefficient is approximately $\eta = 1$. With this assumption, a volume ratio $R_V = 1$ was obtained, suggesting that, in fact, virtually all $PMDS^+$ ions or—to be more precise—all species formed from these ions by dissociation are actually incorporated into the film. In the experiments performed by Brookes et al.,[51] the corresponding sticking coefficient, measured at low power with pressure in the mTorr range, was only 0.2. Possible reasons for this difference are (a) the six orders of magnitude smaller mean free paths lengths in the DBD running at 1 bar, which prevents an easy disappearance of reactive species into the gas phase, and (b) the lack of appreciable kinetic energy of the incoming ions beyond 1 eV.

[9]These results also show that the recombination energy of $Me_3SiOSiMe_2^+$ is <13 eV.

4.3 | Ion oligomerization

In the time span τ_{drift} between generation by reaction (R1) and deposition on the wall, the $PMDS^+$ ion (147 amu) can react with HMDSO. The main product is the heptamethyltrisiloxanyl ion, $HepMTrS^+$, with 221 amu, which formally results from the insertion of a dimethylsilanone unit $Me_2Si{=}O$ (74 amu):

$$Me_3Si–O–SiMe_2^+ + Me_3Si–O–SiMe_3 \rightarrow Me_3Si–O–SiMe_2–O–SiMe_2^+ + (4C, 12H, Si). \quad \text{(R3)}$$

$HepMTrS^+$ has been detected in low-pressure HMDSO plasmas by A. K. Hays (see the citation in reference[22]) as well as by Alexander et al.[29] In a mass spectrometric study, it was formed in 60% of the reactions between $PMDS^+$ and HMDSO, with the remaining 40% resulting in $Si_4O_2C_{11}H_{33}^+$ with 309 amu.[71]

From the relative rate of reaction (R3)—relative to the charge exchange reaction of Ar^+ with HMDSO—provided by Jiao et al.,[71] and the absolute value of the rate coefficient of this reaction reported by Creatore et al.[63] ($4 \pm 2 \times 10^{-10}$ cm^3/s), the rate coefficient of the two-body reaction (R3), k_{R3}, has the value 1.1×10^{-10} cm^3/s. With this figure, the decay time due to reaction (R3), τ_{R3}, of $PMDS^+$ at $x_M = 50$ ppm is 7.6 μs; therefore, the ions will arrive at the film surface largely unreacted within an estimated drift time of 0.5 μs. This figure is taken as a representative value for τ_{drift}, because it would result for $PMDS^+$ ions ($\mu = 2.3$ cm^2·V^{-1}·s[41]) in a cathode fall of 0.3-mm thickness—the approximate position of maximum glow in front of the substrate (Figure 5)—with a cathode drop of 700 V,[17] assuming a constant average field strength ($\rightarrow E = 23$ kV/cm; $E/n = 96$ Td).

At $x_M = 2{,}000$ ppm, however, $\tau_{R3} = 0.19$ μs and the ions will virtually have completely reacted to $HepMTrS^+$, and probably $HepMTrS^+$ will largely be transformed into

16128869, 2020, 11, Downloaded from https://onlinelibrary.wiley.com/doi/10.1002/ppap.202000129 by Technische Informationsbibliothek, Wiley Online Library on [23/01/2025]. See the Terms and Conditions (https://onlinelibrary.wiley.com/terms-and-conditions) on Wiley Online Library for rules of use; OA articles are governed by the applicable Creative Commons License

products with a higher mass, such as non-amethyltetrasiloxanyl, $NMTeS^+$, with 295 amu, and an ion with 309 amu,[29] if the corresponding reactions have rate coefficients similar to k_{R3}. Therefore, the increase of R_V in Figure 8 from 1 to 2.5, with x_M increasing to 2,000 ppm, is not unexpected. However, the near constancy of R_V at 1 up to $x_M = 1{,}000$ ppm and the sudden increase beyond are surprising. A simple kinetic consideration of (R3) shows that the average mass of $PMDS^+$ and $HepMTrS^+$ obtained after 0.5 μs should rise smoothly with x_M, right from the lowest values.

Figure 11 shows the volume ratio R_V and elemental ratio [C]/[Si] as they should be observed if $PMDS^+$ is transformed into $HepMTrS^+$ during a time interval of 0.5 μs. For simplicity, the same drift time, 0.5 μs, has been used in this calculation for both cations, implying the same drift mobilities. Secondary reactions of $HepMTrS^+$ resulting in even larger ions with even smaller [C]/[Si] were neglected, thereby leading to the underestimation of the trends.

As observed from Figure 11, R_V, representing the normalized mass deposited per ion, should increase right from the lowest studied values of x_M, in contrast with what was found experimentally. At present, this discrepancy cannot be explained. It should be noted that the WDX analytical results displayed in Figure 10 do not show an abrupt change at 1,000 ppm. The drop of [C]/[Si] from 2.65 to 2.4 measured for x_M increasing to 2,000 ppm is in an expected order of magnitude if a systematic error of +0.15 (+6%) is assumed. The ratio [O]/[Si] that decreases from nearly 0.8 at $x_M = 50$ ppm and is virtually constant at 0.6 for $x_M \geq 750$ ppm has to be compared with the values of 0.5 for $PMDS^+$ and 0.66 for $HepMTrS^+$; hence, even the trend is in disaccord with what one would expect on the basis of (R3). Possibly, an uptake of atmospheric oxygen takes place in the samples grown with lower x_M, but plausible explanations cannot be given at present.

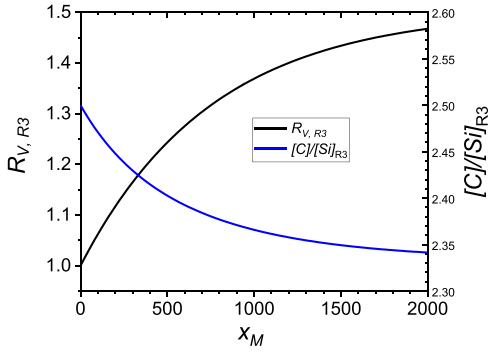

FIGURE 11 Results of model calculations of R_V and [C]/[Si] based on reaction (R3) for a drift time of 0.5 μs and $k_{R3} = 1.1 \times 10^{-10}$ cm^3/s

In the FTIR spectra, the abrupt increase of R_V is accompanied by major changes in the region below 1,000 cm^{-1} (Figure 9c). The assignment of the emerging 767 ± 1 cm^{-1} vibration to ν(Si–C) and ρ(CH_3) in $SiMe_1$ would imply the presence of T units, (Si–O_3), in the SF-DBD deposits.

5 | CONCLUSIONS

Plasma polymerization of HMDSO by means of SF-DBDs in a crossflow of Ar–HMDSO gas mixtures allows the deposition of thin films by a purely ionic deposition mechanism. A comparison of transferred charge with deposited film volume reveals that at small HMDSO fractions of 50 or 100 ppm, film deposition is largely due to $Me_3SiOSi_2^+$ ($PMDS^+$) ions, generated cleanly by Penning ionization in the discharge and drifting within 1 μs or less toward the growing film surface. Due to the large recombination energy in the order of 20 eV, which is released upon neutralization of $PMDS^+$, the resulting PMDS• radical will probably dissociate into reactive fragments from which the film is formed. This mechanism explains the occurrence of vibrations of Si–H and Si–CH_2–Si moieties that are indicative of redistribution reactions of Si ligands, which are similarly known from experiments with hyperthermal $PMDS^+$ ions as well as from photochemical or thermal transformations of siloxanes.

As monomer fractions grow beyond 1,000 ppm, larger ions form the films, which is in qualitative agreement with what is known about the ion chemistry of $PMDS^+$ and HMDSO. It is an open question, however, why the increase of ion mass in the experiment is observed suddenly beyond 1,000 ppm. At present, this behavior cannot be reconciled with a kinetic model. In addition, details of the chemical structure and properties of the films remain to be studied in the future.

We have shown that the investigation of DBD-based plasma deposition processes with the shortest possible residence time is a powerful tool for studying ionic contributions to film deposition. In addition, it may pave the way toward the attainment of enhanced film properties. For the near future, film deposition with a line electrode oriented across the flow direction is planned. With a movable substrate, it will be possible to obtain large-area thin films, which can be used for an in-depth characterization by ellipsometry, XPS, and transmission IR measurements, and for a determination of film properties such as wear and corrosion resistance.

The strong qualitative resemblance of details in IR spectra from SF-DBD and LA-DBD, such as the vibrations of moieties not present in the precursor or in

16128869, 2020, 11, Downloaded from https://onlinelibrary.wiley.com/doi/10.1002/ppap.202000129 by Technische Informationsbibliothek, Wiley Online Library on [23/01/2025]. See the Terms and Conditions (https://onlinelibrary.wiley.com/terms-and-conditions) on Wiley Online Library for rules of use; OA articles are governed by the applicable Creative Commons License

polysiloxanes like Si–H and Si–CH_2–Si, raises the question to what extent ion deposition contributes to film growth in conventional DBDs. This issue, which is of general interest for film deposition by atmospheric-pressure plasma polymerization, will be examined in future studies.

Besides, it should be added that recently performed simulations of DBDs in mixtures of argon with tetramethylsilane are leading to the conclusion that—in analogy to the present case—trimethylsilyl ions can be considered to be mainly responsible for the film formation.[72]

ACKNOWLEDGMENTS

The authors thank Cornelia Steinberg for performing the elemental analyses. They are also grateful for helpful discussions with Dr. Detlef Loffhagen, Prof. Ronny Brandenburg, and Dr. Markus Becker at INP, Greifswald, as well as with Prof. Robert D. Short, Lancaster University, UK, and Dr. Andrew Michelmore, University of South Australia, Australia. Open access funding enabled and organized by Projekt DEAL.

ORCID

Lars Bröcker http://orcid.org/0000-0002-7291-9265
Claus-Peter Klages http://orcid.org/0000-0001-5678-5845

REFERENCES

[1] F. Massines, C. Sarra-Bournet, F. Fanelli, N. Naudé, N. Gherardi, *Plasma Processes Polym.* **2012**, *9*, 1041.
[2] Y. Sawada, S. Ogawa, M. Kogoma, *J. Phys. D: Appl. Phys.* **1995**, *28*, 1661.
[3] K. Schmidt-Szalowski, Z. Rżanek-Boroch, J. Sentek, Z. Rymuza, Z. Kusznierewicz, M. Misiak, *Plasmas Polym.* **2000**, *5*, 173.
[4] A. Sonnenfeld, T. M. Tun, L. Zajíčková, K. V. Kozlov, H.-E. Wagner, J. F. Behnke, R. Hippler, *Plasmas Polym.* **2001**, *6*, 237.
[5] R. Foest, F. Adler, F. Sigeneger, M. Schmidt, *Surf. Coat. Technol.* **2003**, *163–164*, 323.
[6] D. Trunec, Z. Navrátil, P. Sťahel, L. Zajíčková, V. Buršíková, J. Čech, *J. Phys. D: Appl. Phys.* **2004**, *37*, 2112.
[7] M. Hähnel, V. Brüser, H. Kersten, *Plasma Processes Polym.* **2007**, *4*, 629.
[8] R. Morent, N. de Geyter, S. van Vlierberghe, P. Dubruel, C. Leys, E. Schacht, *Surf. Coat. Technol.* **2009**, *203*, 1366.
[9] R. Morent, N. de Geyter, S. van Vlierberghe, P. Dubruel, C. Leys, L. Gengembre, E. Schacht, E. Payen, *Prog. Org. Coat.* **2009**, *64*, 304.
[10] R. Morent, N. de Geyter, T. Jacobs, S. van Vlierberghe, P. Dubruel, C. Leys, E. Schacht, *Plasma Processes Polym.* **2009**, *6*, S537.
[11] L. Zhou, G.-H. Lv, H. Pang, G.-P. Zhang, S.-Z. Yang, *Surf. Coat. Technol.* **2012**, *206*, 2552.
[12] B. Nisol, S. Watson, S. Lerouge, M. R. Wertheimer, *Plasma Processes Polym.* **2016**, *13*, 557.
[13] J. Philipp, A. K. Czerny, C.-P. Klages, *Plasma Processes Polym.* **2016**, *13*, 509.
[14] D. Hegemann, B. Nisol, S. Watson, M. R. Wertheimer, *Plasma Chem. Plasma Process.* **2017**, *37*, 257.
[15] C.-P. Klages, A. K. Czerny, J. Philipp, M. M. Becker, D. Loffhagen, *Plasma Processes Polym.* **2017**, *14*, 1700081.
[16] D. Loffhagen, M. M. Becker, A. K. Czerny, J. Philipp, C.-P. Klages, *Contrib. Plasma Phys.* **2018**, *58*, 337.
[17] D. Loffhagen, M. M. Becker, D. Hegemann, B. Nisol, S. Watson, M. R. Wertheimer, C.-P. Klages, *Plasma Processes Polym.* **2020**, *17*, 1900169.
[18] M. J. Vasile, G. Smolinsky, *J. Electrochem. Soc.* **1972**, *119*, 451.
[19] Y. Segui, B. Ai, *J. Appl. Polym. Sci.* **1976**, *20*, 1611.
[20] W. Möller, M. Schmidt, *Beitr. Plasmaphys.* **1977**, *17*, 121.
[21] A. M. Wróbel, M. R. Wertheimer, J. Dib, H. P. Schreiber, *J. Macromol. Sci. A* **1980**, *14*, 321.
[22] A. M. Wróbel, M. Kryszewski, M. Gazicki, *J. Macromol. Sci. A* **1983**, *20*, 583.
[23] W. Möller, M. Schmidt, R. Seefeldt, R. Wilberg, *Beitr. Plasmaphys.* **1984**, *24*, 629.
[24] K.-D. Schulz, M. Schmidt, *Acta Polym.* **1984**, *35*, 257.
[25] S. Sahli, Y. Segui, S. Hadj Moussa, M. A. Djouadi, *Thin Solid Films* **1992**, *217*, 17.
[26] A. M. Sarmadi, T. H. Ying, F. Denes, *Eur. Polym. J.* **1995**, *31*, 847.
[27] L. Agres, Y. Ségui, R. Delsol, P. Raynaud, *J. Appl. Polym. Sci.* **1996**, *61*, 2015.
[28] M. R. Alexander, F. R. Jones, R. D. Short, *J. Phys. Chem. B* **1997**, *101*, 3614.
[29] M. R. Alexander, F. R. Jones, R. D. Short, *Plasmas Polym.* **1997**, *2*, 277.
[30] F. Benítez, E. Martínez, J. Esteve, *Thin Solid Films* **2000**, *377-378*, 109.
[31] C. Vautrin-Ul, C. Boisse-Laporte, N. Benissad, A. Chausse, P. Leprince, R. Messina, *Prog. Org. Coat.* **2000**, *38*, 9.
[32] S. Zanini, C. Riccardi, M. Orlandi, P. Esena, M. Tontini, M. Milani, V. Cassio, *Surf. Coat. Technol.* **2005**, *200*, 953.
[33] P. Raynaud, B. Despax, Y. Segui, H. Caquineau, *Plasma Processes Polym.* **2005**, *2*, 45.
[34] A. Michelmore, P. M. Bryant, D. A. Steele, K. Vasilev, J. W. Bradley, R. D. Short, *Langmuir* **2011**, *27*, 11943.
[35] M. D. F. Albuquerque, E. Santos Jr., R. R. T. Perdone, R. A. Simao, *Thin Solid Films* **2014**, *564*, 73.
[36] T. Brenner, K. Vissing, *Plasma Processes Polym.* **2020**, *17*, 1900202.
[37] R. Brandenburg, H.-E. Wagner, A. M. Morozov, K. V. Kozlov, *J. Phys. D: Appl. Phys.* **2005**, *38*, 1649.
[38] N. Sewraj, N. Merbahi, J. P. Gardou, P. Rodriguez Akerrata, F. Marchal, *J. Phys. D: Appl. Phys.* **2011**, *44*, 145201.
[39] M. M. Becker, T. Hoder, D. Loffhagen, *J. Phys. D: Appl. Phys.* **2013**, *46*, 355205.
[40] J. Crank, *The Mathematics of Diffusion*, Clarendon Press, Oxford **1975**, p. 47.
[41] M. Schmidt, M. Maass, *Contrib. Plasma Phys.* **1989**, *29*, 197.
[42] P. Nothdurft, G. Riess, W. Kern, *Materials* **2019**, *12*, 550.
[43] R. Holm, *Electric Contacts*, Almquist and Wiksells, Upsalla **1946**, p. 21.
[44] A. E. D. Heylen, *J. Phys. D: Appl. Phys.* **1970**, *3*, 789.
[45] A. E. D. Heylen, *Int. J. Electron.* **1971**, *30*, 121.

16128869, 2020, 11, Downloaded from https://onlinelibrary.wiley.com/doi/10.1002/ppap.202000129 by Technische Informationsbibliothek, Wiley Online Library on [23/01/2025]. See the Terms and Conditions (https://onlinelibrary.wiley.com/terms-and-conditions) on Wiley Online Library for rules of use; OA articles are governed by the applicable Creative Commons License

[46] A. E. D. Heylen, *J. Sci. Instrum.* **1960**, *37*, 251.
[47] A. V. Pipa, R. Brandenburg, *Atoms* **2019**, *7*, 1.
[48] D. R. Anderson, *Analysis of Silicones* (Ed: A. L. Smith), Wiley-Interscience, New York, NY **1974**, p. 247.
[49] G. Socrates, *Infrared and Raman Characteristic Group Frequencies*, John Wiley & Sons, Chichester **2001**.
[50] L. Hanley, E. Fuoco, M. B. J. Wijesundara, A. J. Beck, P. N. Brookes, R. D. Short, *J. Vac. Sci. Technol. A* **2001**, *19*, 1531.
[51] P. N. Brookes, S. Fraser, R. D. Short, L. Hanley, E. Fuoco, A. Roberts, S. Hutton, *J. Electron Spectrosc. Relat. Phenom.* **2001**, *121*, 281.
[52] R. Basner, R. Foest, M. Schmidt, K. Becker, H. Deutsch, *Int. J. Mass Spectrom.* **1998**, *176*, 245.
[53] J. L. Jauberteau, I. Jauberteau, *J. Phys. Chem. A* **2012**, *116*, 8840.
[54] M. Yamane, *J. Phys. Soc. Jpn.* **1960**, *15*, 1076.
[55] K. Beshah, J. E. Mark, J. L. Ackerman, K. Himstedt, *J. Polym. Sci., B: Polym. Phys.* **1986**, *24*, 1207.
[56] J. Cyriac, T. Pradeep, H. Kang, R. Souda, R. G. Cooks, *Chem. Rev.* **2012**, *112*, 535.
[57] Yu. B. Golubovskii, V. A. Maiorov, J. Behnke, J. F. Behnke, *J. Phys. D: Appl. Phys.* **2002**, *35*, 751.
[58] H. Guan, X. Chen, H. Du, A. Paramane, H. Zhou, *J. Appl. Phys.* **2019**, *126*, 093301.
[59] J. L. Jauberteau, I. Jauberteau, *Chem. Phys. Lett.* **2014**, *604*, 116.
[60] S. G. Lias, J. E. Bartmess, J. F. Liebman, J. L. Holmes, R. D. Levin, W. G. Mallard, *J. Phys. Chem. Ref. Data* **1988**, *17*, Suppl. 1.
[61] Yu. P. Raizer, *Gas Discharge Physics*, Springer-Verlag, Berlin **1997**, eq. 2.31.
[62] S. Carles, J. L. Le Garrec, J. B. A. Mitchell, *J. Chem. Phys.* **2007**, *127*, 144308.
[63] M. Creatore, Y. Barell, J. Benedikt, M. C. M. van de Sanden, *Plasma Sources Sci. Technol.* **2006**, *15*, 421.
[64] J. Pola, A. Galíková, A. Galík, V. Blechta, Z. Bastl, Jan Šubrt, A. Ouchi, *Chem. Mater.* **2002**, *14*, 144.
[65] J. Kupčík, Z. Bastl, Jan Šubrt, J. Pola, V. C. Papadimitriou, A. V. Prosmitis, P. Papagiannakopoulos, *J. Anal. Appl. Pyrolysis* **2001**, *57*, 109.
[66] L. Bois, J. Maquet, F. Babonneau, H. Mutin, D. Bahloul, *Chem. Mater.* **1994**, *6*, 796.
[67] G. E. Johnson, D. Gunaratne, J. Laskin, *Mass Spectrom. Rev.* **2016**, *35*, 439.
[68] S. A. Miller, H. Luo, S. J. Pachuta, R. G. Cooks, *Science* **1997**, *275*, 1447.
[69] H. Luo, S. A. Miller, R. G. Cooks, S. J. Pachuta, *Int. J. Mass Spectrom. Ion Processes* **1998**, *174*, 193.
[70] J. W. Denault, C. Evans, K. J. Koch, R. G. Cooks, *Anal. Chem.* **2000**, *72*, 5798.
[71] C. Q. Jiao, C. A. DeJoseph Jr., A. Garscadden, *J. Vac. Sci. Technol. A* **2005**, *23*, 1295.
[72] D. Loffhagen, M. M. Becker, A. K. Czerny, C.-P. Klages, *Plasma Chem. Plasma Process.*, in press. https://doi.org/10.1007/s11090-020-10121-y

How to cite this article: Bröcker L, Perlick GS, Klages C-P. Evidence of ionic film deposition from single-filament dielectric barrier discharges in Ar–HMDSO mixtures. *Plasma Process Polym.* 2020;17: e2000129. https://doi.org/10.1002/ppap.202000129

16128869, 2020, 11, Downloaded from https://onlinelibrary.wiley.com/doi/10.1002/ppap.202000129 by Technische Informationsbibliothek, Wiley Online Library on [23/01/2025]. See the Terms and Conditions (https://onlinelibrary.wiley.com/terms-and-conditions) on Wiley Online Library for rules of use; OA articles are governed by the applicable Creative Commons License